CHIN. PHYS. LETT. Vol. 34, No. 4 (2017) 044101

Radiation Losses in the Microwave X Band in Al-Cr Substituted Y-Type Hexaferrites

D. Basandrai[1,2], R. K. Bedi[3], A. Dhami[2], J. Sharma[2], S. B. Narang[4], K. Pubby[4], A. K. Srivastava[2**]

[1]*Research Scholar, Department of Physics, I. K. Gujral Punjab Technical University, Jalandhar, India*
[2]*Department of Physics, Lovely Professional University, Phagwara, India*
[3]*Principal, Satyam Institute of Engineering & Technology, Amritsar, India*
[4]*Department of Electronic Technology, Guru Nanak Dev University, Amritsar, India*

(Received 6 January 2017)

We present a study on radiation losses in the microwave X band in Al-Cr substituted Y-type hexaferrites, namely $Ba_2Mg_2Al_{x/2}Cr_{x/2}Fe_{12-x}O_{22}$ *(*$x = 0$*, 0.5 and 1.0). The study is performed by means of a vector network analyzer, Fourier transform infrared spectroscopy, a vibrating sample magnetometer and x-ray powder diffraction.* $Ba_2Mg_2Fe_{12}O_{22}$ *hexaferrite shows radiation loss of* -37.25 *dB (99.999% loss) at frequency 9.81 GHz, which can be attributed to its high value of saturation magnetization, i.e., 22.08 emu/g. Moreover, we obtain that magnetic properties have strong influence on the radiation losses.*

PACS: 41.20.Gz, 41.20.Jb, 47.54.Jk DOI: 10.1088/0256-307X/34/4/044101

The ferrites on the basis of crystal structure can be divided into four groups, namely, spinel, garnet, hexaferrite and ortho-ferrite. Such ferrites have many significant applications in magnetic and electrical devices. Due to their nature, resonance and hysteresis loss, the hexaferrites such as Fe_3O_4,[1] $CoFe_2O_4$,[2,3] Z-type,[4] W-type[5,6] and M-type[7] are used as microwave absorbing materials. In addition, Y-type hexaferrites, due to their excellent dielectric losses and conductivity properties, are becoming most popular not only in research but also in technological applications such as EMI shielding, microwave absorbers, defense and aerospace.[8–10] The dielectric and conductivity property of Y-type ferrites are mainly dependent upon the ion distribution and doping elements. The crystal structure of Y-ferrites is rhombohedral, i.e., $R\bar{3}M$, and is mainly constructed from barium hexagonal ferrites and cubic spinal ferrites. The Y-type hexagonal ferrites consist of c-axis interleaving between two layers. One layer contains only oxygen while the other contains Ba substitution for every fourth oxygen. The remaining metallic ions are accommodating at sites of interstices, i.e., tetrahedral (A) or octahedral (B). This arrangement of O and Ba-O forms structural blocks called S and T, respectively.

To control the magnetic properties for better applications in the microwave range, many attempts using different substituent ions have been made such as Zn_2,[11,12] Co_2[13–15] and Ni_2[16] Y-hexaferrites. It has been observed that with Mg-Ni substitution in Y-type strontium hexaferrite, coercivity increases, whereas saturation magnetization and remnant magnetization decrease.[17] Similarly, Li *et al.* showed that with Cu substitution in Y-type hexaferrite, permeability enhances, which significantly affects EM attenuation properties in the microwave region.[18]

The studies have also been carried out on shielding effectiveness properties of Y-type ferrites. Usually, the materials having shielding effectiveness greater than 30 dB are suitable for EMI shielding commercially. In such studies, recently Kim *et al.* have shown 27 dB EMI SE for raw MWCNT–PMMA composites for commercial use in far-field EMI shielding.[19] To enhance the shielding effectiveness more than 30 dB the present study has been carried out with aluminum and chromium substituted Y-type hexaferrites, i.e., $Ba_2Mg_2Al_{x/2}Cr_{x/2}Fe_{12-x}O_{22}$ ($x = 0$, 0.5 and 1.0) using the sol-gel method. The influence of Al and Cr ions on the structural and magnetic properties of $Ba_2Mg_2Al_{x/2}Cr_{x/2}Fe_{12-x}O_{22}$ ($x = 0$, 0.5 and 1.0) has been investigated systematically.

The synthesis of an Al-Cr substituted Y-type barium hexaferrite has been carried out through a sol-gel method using AR grade metal nitrates without any purification. An equal stoichiometry of metal nitrates is put into a clean beaker and is dissolved in distilled water. Ammonia solution has been used to maintain the pH = 7. The solution is heated at 80–85℃ for 4–6 h under continuous magnetic stirring, during which it turns into a brown colored gel. Then, the hot plate is used to heat the precursor at 280–300℃ for 3 h. Pre-sintering has been carried out at 500℃ for 2 h at a rate of 23℃/min to remove impurities. Then the precursor material is sintered at 900℃ at a rate of 23℃/min for 5 h to obtain the calcined precursor. The precursor is further sintered at 900℃ for 6 h. Finally the powder is sintered at 1000℃ for 5 h.

Attached functional groups have been analyzed

**Corresponding author. Email: srivastava_phy@yahoo.co.in
© 2017 Chinese Physical Society and IOP Publishing Ltd

with Fourier transform infrared spectrometry (FTIR interferometer IR prestige-21 FTIR (model-8400 S)) in the range of 400–4000 cm^{-1} by making sintered product pallets with 2 mg of ferrite powder mixed with powdered KBr in the ratio 1:100 by weighing to ensure uniform dispersion. Magnetic properties have been studied with a vibrating sample magnetometer (Lakeshore 7410). Microwave studies have been carried out with a vector network analyzer (Agilent 8722ES). For the radiation loss measurements, the sample has been molded in a rectangular shape using an aluminum die. To increase the strength of pellet, polyvinyl alcohol (PVA) is used as a hardener. X-ray diffraction analysis of powder samples is carried out with a Bruker AXS D8 Advance x-ray diffractometer in the range of 20–80° using Cu Kα radiation.

The XRD patterns of $Ba_2Mg_2Al_{x/2}Cr_{x/2}Fe_{12-x}O_{22}$ ($x = 0$, 0.5 and 1.0) are shown in Fig. 1.

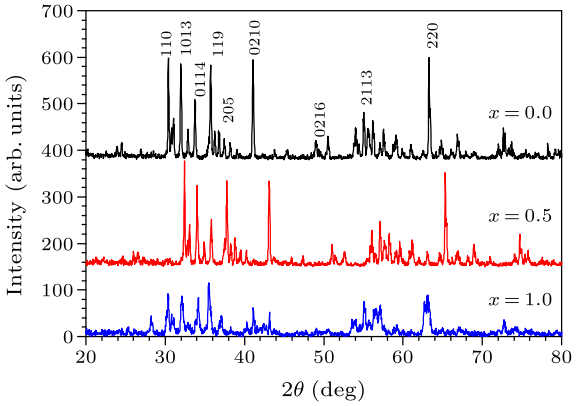

Fig. 1. XRD patterns of hexaferrite $Ba_2Mg_2Al_{x/2}Cr_{x/2}Fe_{12-x}O_{22}$ at different compositions ($x = 0$, 0.5 and 1).

Table 1. Values of different parameters calculated for hexaferrite, i.e., lattice constant a, lattice constant c, cell volume v, cell size χ, and strain δ.

Sample	a (Å)	c (Å)	v (Å^3)	χ (nm)	δ
$x = 0$	5.83	43.86	1291.8	52	0.2×10^{-3}
$x = 0.5$	5.85	44.432	1317.12	69	0.3×10^{-3}
$x = 1$	5.87	44.76	1336.54	25	1.8×10^{-3}

The XRD patterns for these compositions confirm the formation of pure Y-type hexaferrite.[20] The average crystallite size of the hexaferrite is calculated by the Scherrer formula

$$D = \frac{k\lambda}{\beta\cos\theta},$$

where D is the crystallite size, $k = 0.89$ is a dimensionless shape factor and is related to the shape of the crystallites, and λ is the x-ray wavelength (1.54 Å). The lattice parameters (a and c) and cell volume (V) are calculated by

$$\frac{1}{d_{hkl}^2} = \frac{4}{3}\left[\frac{h^2+hk+k^2}{a^2}\right] + \frac{l^2}{c^2},$$
$$V = 0.8666a^2c,$$

where d is the inter-planer spacing, and h, k and l are the corresponding Miller indices. The calculated lattice parameters, average grain size and cell volume are listed in Table 1.

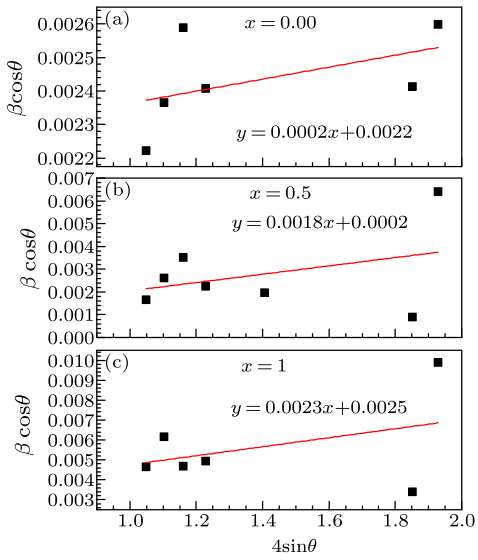

Fig. 2. Plots of $4\sin\theta$ versus $\beta\cos\theta$ for $Ba_2Mg_2Al_{x/2}Cr_{x/2}Fe_{12-x}O_{22}$ for (a) $x = 0$, (b) $x = 0.5$ and (c) $x = 1.0$.

Strain ε caused by distortion and crystal imperfection in the powder is calculated using the Williamson–Hall (W-H) method,

$$\varepsilon = \frac{\beta}{4\tan\theta}. \quad (1)$$

For the Lorentzian peak shape, the W-H analysis is derived from

$$\beta\cos\theta = \left[\frac{k\lambda}{D}\right] + 4\varepsilon\sin\theta. \quad (2)$$

The variation of $4\sin\theta$ versus $\beta\cos\theta$ is shown in Fig. 2.

Strain is calculated from the slope and the crystalline size is estimated from the y-intercept of the linear fit.[21,22] With the increase of the concentration of dopants, strain is also increased. This may be due to the low calcination temperature, which suggests that the powder is experiencing strain.

Figure 3 shows the room-temperature M–H loops for all the samples. The saturation magnetization M_s, coercivity H_c and retentivity of synthesized compounds have been obtained from the M–H loops. For $x = 0$ and 0.5, the coercivity is very low, i.e., 16.66 Oe and 27.77 Oe, respectively, indicating soft magnetic materials. Saturation magnetization (at $x = 0$, M_s = 19.85 emu/g and $x = 1$, M_s = 22.08 emu/g) and remanence magnetization (at $x = 0$, M_r = 1.20 emu/g and $x = 1$, M_r = 8.36 emu/g) increase with the Al-Cr substitution, and this behavior can be attributed to the occupation of Al, Cr at A and B sites in the Y-type hexaferrite structure. Fe ions reside in seven

different lattice site having up and down spins, which contribute to the resultant magnetic moment of the Y-type hexaferrite. The resultant magnetic moment increases due to the replacement of some down-spin Fe ions with Al-Cr ions.

The magnetic anisotropy constant K, which depends upon coercivity H_c, is calculated by

$$H_c = \frac{2K}{\mu_0 M_s}, \tag{3}$$

where M_s is the saturation magnetization, and μ_0 is the permeability of the free space. The calculated values of coercivity H_c and magnetic anisotropy constant K are shown in Table 2.

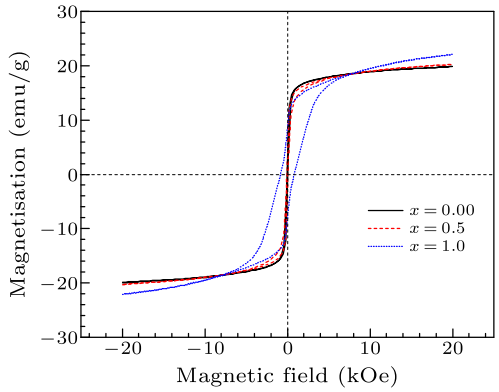

Fig. 3. Hysteresis loop plots for all the samples.

Table 2. Values of coercivity H_c, saturation magnetization, remanence magnetization and magnetic anisotropy constant K (in units of H·A^2/kg with H standing for Henry, A for Ampere and kg for kilogram) with substitution.

Sample	H_c (Oe)	M_s (emu/g)	M_r (emu/g)	K
$x = 0$	16.66	19.85	1.20	0.02
$x = 0.5$	27.77	20.21	1.30	0.03
$x = 1.0$	805	22.08	8.36	0.89

Two peaks have been obtained for the sample $Ba_2Mg_2Al_{x/2}Cr_{x/2}Fe_{12-x}O_{22}$ in the range of 400–600 cm^{-1}, indicating the formation of Y-type hexaferrites.

A rectangular aluminum die has been used to convert the sample in rectangular shape for radiation loss measurement. The multiple reflection from hexaferrite particles and entrapping of EM wave inside the hexaferrite materials are the reasons for the loss of EM waves. In agreement with the theory of absorbing wall, normalized input impedance can be calculated by [23]

$$Z = \sqrt{\frac{\mu^*}{\varepsilon^*}} \tanh\left(j\frac{2\pi t}{\lambda}\right)\sqrt{\mu^*\varepsilon^*},$$

where $\varepsilon*$ is the complex permittivity, Z is the normalized input impedance, $\mu*$ is the complex permeability, t is the thickness of the sample pellet, and λ is the wavelength. The radiation losses can be calculated by[23]

$$\text{Radiation loss(dB)} = 20\log\left(\frac{Z-1}{Z+1}\right).$$

The dependence of the calculated reflection loss with the X band frequencies (8–12.3 GHz) for synthesized samples is shown in Fig. 4. A distinct pattern reveals that the reflection loss depends on the presence of doping and the magnetic properties of hexaferrite. The sample with $x = 0$ shows the maximal reflection loss (−37.25 dB) because of its low value of saturation magnetization (19.85 emu/g) and low value of coercivity. The sample with $x = 1.0$ shows the minimal reflection losses (−2.53 dB) due to its high value of saturation magnetization (22.08 emu/g) and high value of coercivity (805 Oe).

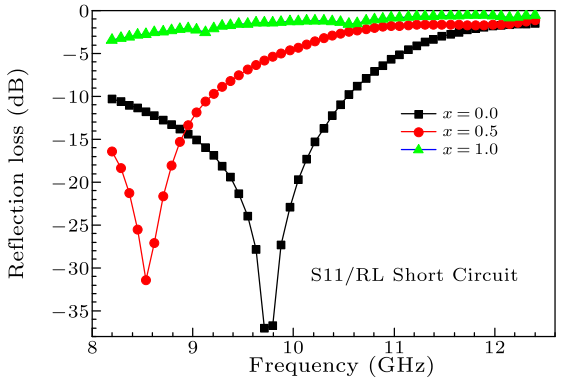

Fig. 4. Reflection loss for composite samples on the frequency in the range of 8–13.0 GHz.

The Nicholson–Ross–Weir method was employed to find the values of permittivity and permeability. The results are plotted in Fig. 5. Major variations in the values of permittivity and permeability have been found from the samples. The sample with $x = 0$ shows a minimum of permeability but a maximum of permittivity, while the sample with $x = 1.0$ shows a maximum of permeability but a minimum of permittivity for the same frequency range. For the sample with $x = 0$, permeability increases with the frequency while permittivity decreases with the increase of the frequency. The value of permittivity shows variation from 6.2 to 6.6 with the increase of frequencies increasing from 8 GHz to 12.5 GHz. Permittivity is a function of the induced polarization due to the change in voltage in a material. For the undoped sample, permittivity was found to be higher in comparison with the doped sample in the same frequency range. This decrease can be attributed to the substitution of Al-Cr ions in the material which reduces the dipole and interfacial polarization. The decrease in permittivity can also be understood with regard to conductivity, which decreases with substitution.[24] Also, permittivity shows dependence on frequency. It has been observed that permittivity decreases with the

increase of the frequency, which is a typical behavior of ferrites.[25] Dielectric loss for the undoped sample has been found nearly to zero. However, 9% increase in dielectric loss has been found with the substitution of Al and Cr. This increase is very useful in absorption applications because high loss suggests high energy dissipation. Dielectric losses also show strong dependence on frequency. The real part of permeability also increases with the Al-Cr substitution which may be due to the decrease of grain boundaries and porosity of the samples with substitution. This induces a low reluctance to magnetic domain motion by producing high demagnetizing field. Also permeability increases with the frequency. Magnetic loss, i.e., imaginary permeability, arises due to the lack between magnetization and applied field. Imaginary permeability decreases with the doping concentration. No dependence on frequency has been observed in the case of imaginary permeability.

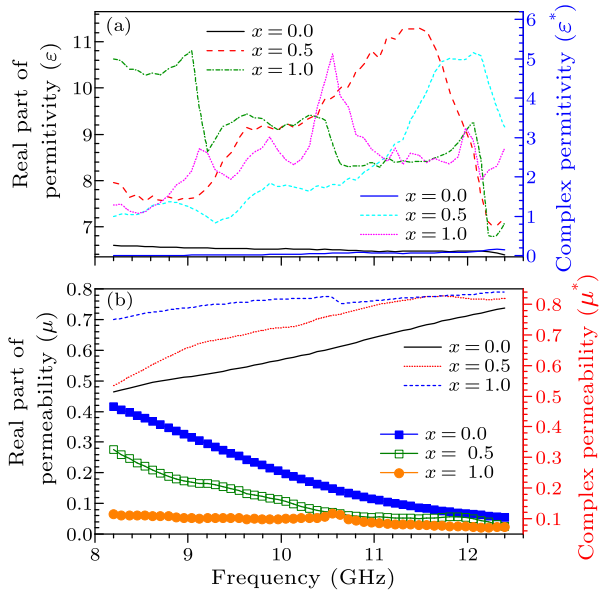

Fig. 5. Real part and complex part of (a) permittivity and (b) permeability for reflection losses.

In summary, the Y-type nano-hexaferrite has been synthesized using the sol-gel technique and has been characterized by using FTIR, VNA,VSM and XRD. Presence of two prominent peaks near 550–600 cm^{-1} to 400–600 cm^{-1} in FTIR indicates the formation of hexaferrite. From VSM analysis, it is found that with the increasing amount of co-dopants Al-Cr, the saturation magnetization, coercivity and retentivity increase. Consecutive peaks of radiation loss of about −37.25 dB have been found in the plots. Hence, a prepared material has good reflection loss values, which makes the material possible for the communication and microwave devices.

References

[1] Huang X, Chen Y, Yu J, Zhang J, Sang T, Tao G and Zhu H 2015 *J. Mater. Sci.: Mater. Electron.* **26** 3474
[2] Huang X, Zhang J, Rao W, Sang T, Song B and Wong C 2016 *J. Alloys Compd.* **662** 409
[3] Huang X, Zhang J, Wang W, Sang T, Song B, Zhu H, Rao W and Wong C 2016 *J. Magn. Magn. Mater.* **405** 36
[4] Li B, Shen Y, Yue Z and Nan C 2007 *J. Magn. Magn. Mater.* **313** 322
[5] Huang K, Xiansong L, Shuangjiu F, Jiangying Y, Xiaofei N, Farui L and Huang X 2016 *Mater. Technol.* **31** 10
[6] Huang K, Xiansong L, Shuangjiu F, Zhanjun Z, Jiangying Y, Xiaofei N, Farui L and Xing H 2015 *J. Magn. Magn. Mater.* **379** 16
[7] Huang X, Zhang J, Liu Z, Sang T, Song B, Zhu H and Wong C 2015 *J. Alloys Compd.* **648** 1072
[8] Smit J and Wijn H P J 1959 *Ferrites* (Eindhoven: Philips' Technical Library)
[9] Shen S, Chai Y and Sun Y 2015 *Sci. Rep.* **5** 8254
[10] Ohlan A, Singh K, Chandra A, Singh V N and Dhawan S K 2009 *J. Appl. Phys.* **106** 044305
[11] Kamba S, Goian V, Savinov M, Buixaderas E, Nuzhnyy D, Marys ko M, Kempa M, Bovtun V, Hlinka J and Knizek K 2010 *J. Appl. Phys.* **107** 104109
[12] Hirose S, Haruki K, Ando A and Kimura T 2015 *J. Am. Ceram. Soc.* **98** 2104
[13] Costa M, Junior G P and Sombra A 2010 *Mater. Chem. Phys.* **123** 35
[14] Ali I, Islam M, Ashiq M N, Khan H M, Iqbal M A and Najam U H M 2014 *Mater. Res. Bull.* **49** 338
[15] Ali I, Islam M, Ashiq M N, Iqbal M A, Awan M and Naseem S 2014 *J. Alloys Compd.* **599** 131
[16] Ifran M, Islam M, Ali I, Iqbal M A, Karamat N and Khan H M 2014 *Curr. Appl. Phys.* **14** 112
[17] Farzin Y A, Mirzaee O and Ghasemi A 2014 *J. Magn. Magn. Mater.* **371** 14
[18] Chua M J, Yang Z H and Li Z W 2014 *J. Magn. Magn. Mater.* **368** 19
[19] Kim H M, Kim K, Lee C Y, Joo J, Cho S J, Yoon H S, Pejakovic D A, Yoo J W and Epstein A J 2004 *Appl. Phys. Lett.* **84** 589
[20] Bai Y, Zhou J, Gui Z, Yue Z and Li L 2003 *Mater. Sci. Eng.* B **99** 266
[21] Anthonyraj C, Muneeswaran M, Gokul R, Giridharan N V, Sivakumar V and Senguttuvan G *J Mater Sci: Mater Electron* **26** 49
[22] Sarma H and Sarma K C 2014 *Int. J. Sci. Res. Publ.* **4** 3
[23] Kaur T, Kumar S, Sharma J and Srivastava A K 2015 *Beilstein J. Nanotechnol.* **6** 1700
[24] Li Q, Yin X, Duan W, Kong L, Liu X, Cheng L and Zhang L 2014 *J. Eur. Ceram. Soc.* **34** 2187
[25] Aen F, Ahmad M and Rana M U 2013 *Curr. Appl. Phys.* **13** 41